Pressure-Induced Fluorescence Enhancement of the BSA-Protected Gold Nanoclusters and the Corresponding Conformational Changes of Protein

ARTICLE *in* THE JOURNAL OF PHYSICAL CHEMISTRY C · DECEMBER 2012

Impact Factor: 4.77 · DOI: 10.1021/jp309175k

8 AUTHORS, INCLUDING:

Yuqing Wu
Jilin University
124 PUBLICATIONS **1,695** CITATIONS
SEE PROFILE

Kai Wang
Tongji Medical University
96 PUBLICATIONS **770** CITATIONS
SEE PROFILE

Bo Zou
Harbin Institute of Technology
189 PUBLICATIONS **2,475** CITATIONS
SEE PROFILE

THE JOURNAL OF PHYSICAL CHEMISTRY C

Article

pubs.acs.org/JPCC

Pressure-Induced Fluorescence Enhancement of the BSA-Protected Gold Nanoclusters and the Corresponding Conformational Changes of Protein

Min Zhang,[†] Yong-Qiang Dang,[†] Tian-Ying Liu,[†] Hong-Wei Li,[†] Yuqing Wu,*[,†] Qian Li,[‡] Kai Wang,[‡] and Bo Zou*[,‡]

[†]State Key Laboratory of Supramolecular Structure and Materials, Jilin University, No. 2699, Qianjin Street, Changchun 130012, P. R. China

[‡]State Key Laboratory of Superhard Materials, Jilin University, No. 2699, Qianjin Street, Changchun 130012, P. R. China

ABSTRACT: We investigated the pressure-induced fluorescence enhancement of BSA-protected gold nanoclusters, AuNCs@BSA, and the corresponding conformational changes of ligand protein by *in situ* fluorescence and IR spectral measurements. It is documented that the fluorescence enhancement of AuNCs@BSA is essentially attributed to the conformational changes of the ligand, which undergoes substantial secondary and tertiary structural changes. Under compression BSA loses more buried α-helical structure, while it changes oppositely in the AuNCs@BSA as the protein adopts a more flexible conformational state at the boundary surface of gold nanoclusters. The present work will be helpful to understand the fundamental mechanism and to reveal the important factors of ligands in nanoclusters, which are hope to improve the luminescence efficiency of gold nanoclusters in final.

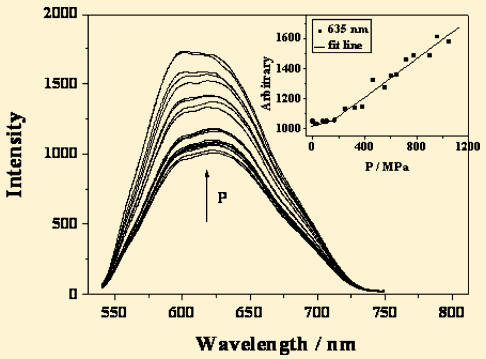

1. INTRODUCTION

Noble metal (gold, silver) nanoclusters (NCs), composed of a few to roughly a hundred atoms, are a new type of luminescent nanomaterials that have attracted a great interests recently.[1−4] Metal NCs typically have diameters below 2 nm and therefore in size locate between isolated atom and larger nanoparticles. For dimensions approaching the Fermi wavelength of electrons, the continuous density of states breaks up into discrete energy levels leading to the observation of dramatically different optical, electrical, and chemical properties as compared to nanoparticles.[1,4,5] A distinct feature is their strong photoluminescence, in combining with good photostability, large Stokes shift, and high emission rates. Moreover, recent advances have enabled facile synthesis of water-soluble fluorescent metal NCs with different ligands and tunable emission colors in various biocompatible scaffolds, establishing them as a new class of ultrasmall fluorophores for applications in biological systems.[6−8]

The conjugation of protein with nanoclusters not only affords stabilization to the system;[2,5] also, the bright emission of clusters in protein templates enables them well exploited for biolabeling.[1,9,10] Moreover, a fundamental understanding of the conformational behavior of ligand proteins in the NCs conjugates is of critical importance in developing the bio-applicable nanomaterials. Currently, several mechanisms have been proposed to explain the emission properties of ultrasmall metal NCs.[2,11−16] However, unlike QDs, no fixed mechanism is currently accepted to explain the luminescence from the metal NCs as the mechanism may be different for metal NCs with different sizes, coating ligands, or even when they are prepared by different synthesis routes.

High pressure has been introduced into studies on photophysical and photochemical properties of luminescent compounds.[17,18] One aspect of pressure tuning is related to the relative energies of bonding and antibonding orbitals to intra- and intermolecular interactions. The second aspect of pressure tuning is related to bulk properties of matter such as volume, viscosity, and dielectric constant to molecular properties. Pressure effects on molecular group symmetry, energy gap, spatial arrangement of ligands, and potential energy surfaces are qualitatively considered for the drastic pressure-induced change in luminescence intensity. Besides the effect on the electronic state and the configuration of the molecules, pressure can also affect phase transitions and crystal lattices of compounds, which leads to significant changes in second harmonic generation (SHG) and luminescent properties. In considering the advantageous photophysical properties of metal NCs over the conventional fluorophores as organic dyes and fluorescent proteins,[19−21] it is then not surprising that high-pressure investigations on nanomaterials are developed in parallel to the fast growth of nanosciences either to better understand the properties of nanomaterials or to provide alternative methods for nanostructuration. Pressure-induced shape changes of nanocrystal were first evidenced in 1996 for crystalline silicon.[22]

Received: September 15, 2012
Revised: December 17, 2012
Published: December 17, 2012

Some years later, San-Miguel underlined the investigation through pressure cycling of the wurtzite to the rocksalt transition of CdSe, allowing to propose a mechanism of sliding planes to relate both structures.[23] In the case of CdSe nanocrystal, the upstroke transition pressures were shifted toward higher pressures when reducing the size of the nanocrystal. All these examples serve to illustrate the potential of high pressure for the understanding of fundamental phenomena and mechanism and finally for the elaboration of new nanomaterials.[24,25]

In the present study we applied *in situ* fluorescence and Fourier transform infrared (FTIR) spectroscopy to investigate the pressure-induced optical properties and ligand conformational changes of BSA-protected gold nanoclusters (AuNCs@BSA) in aqueous solutions. The aim is to understand the fundamental optical phenomena and mechanism, and essentially the crucial factors of ligands in nanoclusters, and finally to stimulate more experimental and theoretical researches on the atomic level design of luminescent metal nanoparticles for promising optoelectronic and other applications at the atomic level. We also expect the current *in situ* spectral measurements will be helpful to improve the ligand of nanoclusters landing to improve their optical properties.

2. EXPERIMENTAL PROCEDURES

2.1. Materials. Bovine serum albumin (BSA, fraction V), purchased from Sigma, is used without further purification. The stock solution of BSA is prepared in 0.01 M phosphate buffer solution (PBS) of pH 7.0, containing 0.01 M NaCl. PB solutions with other pH values used in the experiment are prepared by adding concentrated HCl or NaOH to the prepared one. The final concentration of BSA is measured photometrically by using a molar absorptivity of 44 000 mol^{-1} cm^{-1} at 278 nm. The $HAuCl_4{\cdot}3H_2O$ and trisodium citrate are purchased from Beijing Chemical Company. All other reagents are of analytical reagent grade and used as received. The water used is purified through a Millipore system.

2.2. Synthesis of BSA-Protected Gold Nanoclusters (AuNCs@BSA). AuNCs@BSA are prepared according to previously reported methods,[5] which can be summarized as 5 mL aqueous solution of $HAuCl_4$ (10 mM, 37 °C) is added to BSA solution (5 mL, 50 mg/mL, 37 °C) under vigorous stirring. Two minutes later, 0.5 mL of NaOH solution (1 M) is introduced, and the mixture is incubated at 37 °C for 12 h with constant stirring. The color of the solution changes from light yellow to light brown first and then to deep brown. The reaction is completed in ~12 h, as confirmed by time-course measurements of the fluorescence evolution. Then the solution are dialyzed with a 10 kDa cutoff dialysis bag extensively against doubly distilled water to remove all small molecular impurity first and consequently isolated by using a commercially supplied Sephadex G-75 gel column (supplied by Pharmacia) to remove the excessive BSA.[26] Finally, it is subjected to freeze-drying to obtain the powder of AuNCs@BSA for further characterization and/or quantitative investigations.

2.3. Instruments. UV−vis absorption spectra are recorded with a Shimadzu UV-3600 spectrophotometer for solutions with concentration of 10 mg/mL AuNCs@BSA contained in 1 cm × 1 cm quartz cuvettes (4 mL volume). The high-resolution transmission electron microscopy (HRTEM) images are observed by JEM-2200FS (Jeol Ltd. Japan) equipped with a thermally assisted field-emission gun operated at an accelerating voltage of 200 kV. X-ray photoelectron spectroscopy (XPS) measurements are carried out on an ESCALAB 250 spectrometer with a monochromic X-ray source (Al Kα line, 1486.6 eV), and the charging shift was corrected by the binding energy of C 1s at 284.6 eV. MALDI-TOF mass spectrometry was performed on an Autoflex III MALDI-TOF mass spectrometer (sinapinic acid is used as the matrix for MALDI, and tetrafluoroacetic acid is added to enhance the ionization).

2.4. *In Situ* Measurement of Pressure-Induced Fluorescence Spectra. The high-pressure measurements of fluorescence spectra are performed by using a symmetric diamond anvil cell (DAC) with 1 mm diamond culets. A T301 stainless steel gasket is preindented by the diamond anvils with a thickness of 0.24 mm and then drilled to produce a 0.4 mm diameter cavity as the sample chamber. The solution is introduced into the chamber, and a small ruby chip is also placed in the chamber for *in situ* pressure calibration. By observing the separation and widths of both R1 and R2 lines of ruby fluorescence, we confirm that the hydrostatic conditions are according to the shift of the R1 line of the ruby fluorescence; the value of the pressure can be determined. To achieve high signal-to-noise ratio a high concentration of AuNCs@BSA (40 mg/mL) is used for the high-pressure spectral measurement. However, such a high concentration may cause self-absorption or inner filter effect in fluorescence measurement, which can be ignored as we focus on the spectral difference. The spectra are recorded in the wavelength range of 540−750 nm upon excitation at 490 nm, and the presented spectra are the representative sets of three measurements. The choice of 490 nm as the excitation wavelength is to avoid the self-absorption of BSA.

2.5. *In Situ* Measurements of Pressure-Induced IR Spectra. High pressures for IR spectra are generated in a diamond anvil cell (Diacell Lever DAC-Mini A65000), where the pressure is increased with a screw mechanism. The solution is placed in a 0.3 mm diameter hole on a 0.025 mm thick stainless steel gasket mounted on a diamond anvil cell. $BaSO_4$ is used as an internal pressure calibrant, and the pressures are determined by the frequency changes in the IR absorption band at around 983 cm^{-1} for it. FT-IR spectral measurements at ambient and elevated pressure are all performed at a Bruker Vertex 80 V FT-IR spectrophotometer equipped with a liquid nitrogen-cooled mercury cadmium telluride (MCT) detector. For each spectrum, 512 interferograms are coadded for a spectral resolution of 2 cm^{-1}.

An IR spectrum of water vapor is subtracted from all spectra before smoothing. The data manipulation comprising the subtraction, truncation, and baseline corrections of the IR spectra are performed based on a previously described method.[27,28] Spectral smoothing is performed with RAZOR software (Spectrum Square Associates Inc., Ithaca, NY), which also runs under GRAMS/386 (Galactic Inc. Corp.). The smoothing uses the method of maximum entropy and assumes a Gaussian line shape of 20 cm^{-1} full width at half-height. Curve fitting with Gaussian functions is performed using Origin software.

3. RESULTS

3.1. Characterization of AuNCs@BSA. The prepared gold nanoclusters are assayed first by the high-resolution transmission electron microscopy (HRTEM), where the Au cores are obviously observed (Figure 1A). In addition, XPS has also been used to determine the content and oxidation states of

dx.doi.org/10.1021/jp309175k | J. Phys. Chem. C 2013, 117, 639−647

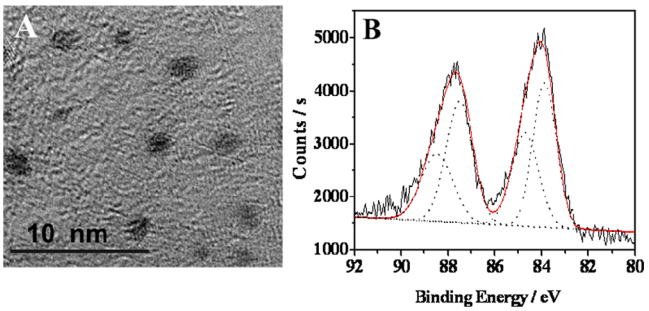

Figure 1. (A) High-resolution TEM image and (B) XPS spectrum of AuNCs@BSA.

metal in samples. The binding energy of Au $4f_{7/2}$ at ~84.0 eV can be deconvoluted into two distinct peaks at 83.8 and 85.0 eV (Figure 1B), respectively, being assigned to Au(0) and Au(I) and confirming the existence of Au−Au interaction.[5,29,30]

The optical properties of metal nanoparticles are generally dominated by the surface plasmon resonance. However, when the size is reduced to the subnanometer scale, metal clusters are too small to support plasmon and a transition from metal to molecule. Instead of forming continuous densities of states and behaving as conductors, these few atom metal NCs generally exhibit discrete energy levels.[2,9] The redissolved AuNCs@BSA powders in solution are pale brown and emit at 635 nm under 490 nm excitation (Figure 2A), being close to the fluorescence emission band reported by the first approach of BSA-protected AuNCs.[5] Similarly, we assigned them as the predominance of 25 gold atoms in core, that is, Au_{25}NCs@BSA. Such conclusion is further confirmed by the MALDI-TOF mass spectrum in Figure 2B. Based on the central position of half-bandwidth, a peak at ~71.1 kDa is assigned for AuNCs@BSA. The difference between it and BSA corresponds to 25 gold atoms in the core, while the broad shape of it attributes to a wide distribution of gold atoms there, being consistent with the HRTEM result in Figure 1A.

Well-defined metal NCs are also expected to possess characteristic absorption features and can be distinguished from each other by their absorption profiles.[31] However, unlike the absorption spectra of larger Au nanoparticles, the UV−vis absorption spectrum of AuNCs@BSA in Figure 2A indicates only weak surface plasmon resonance (SPR) absorption in the range 400−600 nm. Although small molecule protected Au cluster generally has characteristic absorbance features,[32,33] the SPR absorption spectrum of the reported AuNCs@BSA only has a weak broad absorbance peak between 400 and 600 nm. Such result is consistent with the previously reported BSA protected gold nanoclusters,[5,34−36] indicating an NC diameter less than 2 nm.[31,36]

In addition, based on the reported method,[37] the quantum yield of Au_{25}NCs@BSA is found to be 5%. The nature of BSA in the Au_{25}NCs@BSA is then studied by FT-IR and CD spectra, which give features mainly resulting from the BSA ligand (Figure 3).[26] Furthermore, the enlarged IR spectrum of the Au_{25}NCs@BSA in low wavenumber region is compared with that of pure BSA, showing somewhat differences between them at secondary structures in the amide I region. It is necessary to note that an efficient separation technique[26] has been employed to exclude the excessive BSA in the synthesis system before we give further interpretations of its IR spectra. That is, the possible effects of the conformational behavior of protein beside the conjugates have been excluded in the IR spectra of AuNCs@BSA. To further check the conformational differences between BSA and AuNCs@BSA, CD spectra of them are performed (Figure 3B). For the AuNCs@BSA, the peaks are observed at 208 and 222 nm, indicating that some conformational changes indeed occur when BSA is capped on the AuNCs surface as a ligand.

3.2. Pressure-Induced Fluorescence Enhancement of AuNCs@BSA. The pressure-induced changes in optical property of AuNCs@BSA are monitored by checking the *in situ* fluorescence spectra in solution at intervals of pressure. Figure 4 shows the emission spectra of AuNCs@BSA measured with pressure elevation upon excitation at 490 nm. As shown, at room temperature and atmospheric pressure, the AuNCs@BSA displays a fluorescence emission spectrum with a maximum at 635 nm, according a dominant cluster size of Au25.[5] The broad emission with a shoulder at 595 nm should attribute to the different excited state exist in AuNCs@BSA.[12] The positions of these peaks are found almost constant, but obvious intensity enhancements of the emission are observed for the AuNCs@BSA with pressure elevation. Being divided by the fluorescence spectrum measured at atmospheric condition, the fluorescence intensities at 635 and 595 nm are enhanced 70.1 and 80.3%, respectively, corresponding to the pressure of 1050 MPa (Figure.4). Furthermore, the inset in Figure 4 shows the plot of the fluorescence intensity at 635 nm versus pressure. Under curve fitting, the pressure-induced fluorescence changes can be divided into two stages, i.e., $P < 250$ MPa and $P > 250$ MPa. At the first stage only slight change is observed for the

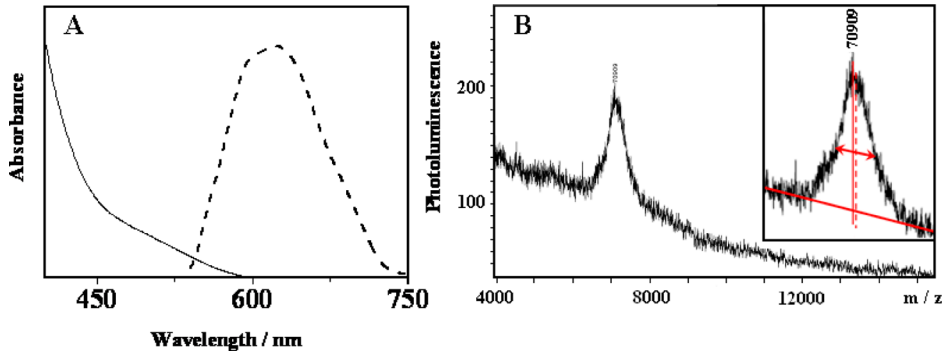

Figure 2. (A) Fluorescence emission (dotted line, excitation at 490 nm) and UV−vis absorption (solid line) spectra of AuNCs@BSA in aqueous solution. (B) MALDI-TOF mass spectrum and its peak enlargement (inset) of the presented AuNCs@BSA.

dx.doi.org/10.1021/jp309175k | J. Phys. Chem. C 2013, 117, 639−647

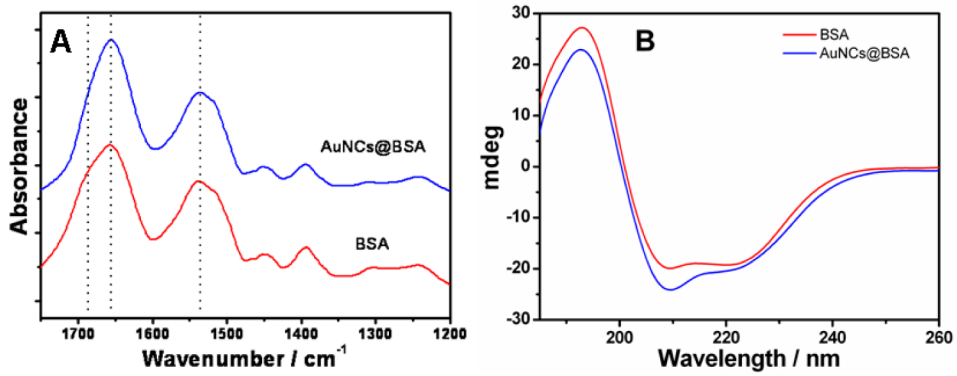

Figure 3. (A) FT-IR spectra in 1750−1200 cm^{-1} region and (B) CD spectra of BSA and AuNCs@BSA.

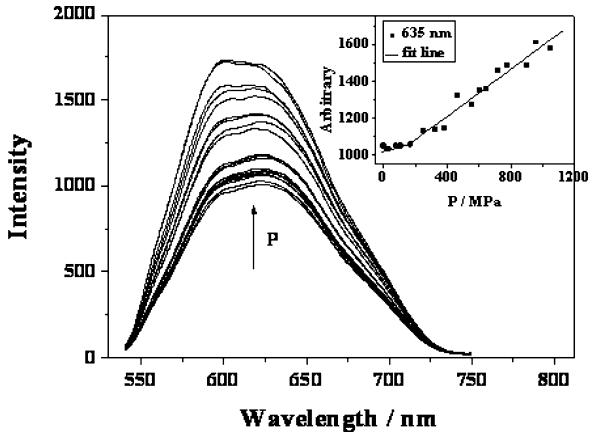

Figure 4. Pressure-dependent fluorescence spectra of AuNCs@BSA (λ_{ex} = 490 nm). Arrow represents the direction of pressure changes from 0.1 to 1050 MPa. Inset: plots of fluorescence intensity at 635 nm of AuNCs@BSA against pressure.

fluorescence intensity, but it increases almost linearly with applied pressure since 250 MPa.

In considering the advantages of 2D correlation analysis in determining the subtle structural changes in highly overlapping bands, here, it is also applied to the pressure-dependent fluorescence spectra of AuNCs@BSA. 2D correlation contour maps in Figure 5A,B are constructed from the spectra measured at pressure ranges of 250−1050 MPa. The synchronous 2D contour map shows an intense autopeak centered at around 600 nm. Unfortunately, the involved two bands cannot be

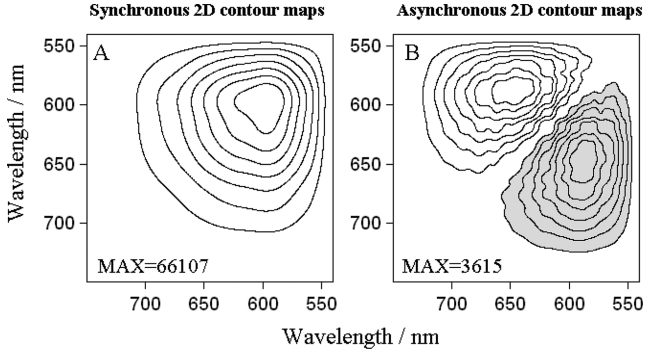

Figure 5. (A) Synchronous and (B) asynchronous 2D contour maps for AuNCs@BSA constructed from pressure-dependent fluorescence spectra measured between 250 and 1050 MPa.

deconvoluted well in the synchronous spectrum. However, the asynchronous 2D correlation spectrum in Figure 5B shows two separated cross-peaks clearly, which is antisymmetric with respect to the diagonal line. The cross-peak is developed only when the intensities of two spectral features change out of phase with each other.[38] The splitting of two peaks at 595 and 635 nm in Figure 5B again indicates the fluorescence bands originate from two distinctively different excited states of Au core.[12] Meanwhile, according to the rule put forward by Noda,[38] the intensity of the band at 635 nm varies from relatively lower pressure than that of the band at 595 nm, indicating that the former state may be more sensitive to pressure than the latter.

3.3. Pressure-Induced Conformational Changes of Ligand BSA As Revealed by IR Spectra. Following the above observation of the fluorescence spectra, it can be suggested that the ligand BSA may play an important role in the pressure-induced fluorescence enhancement of AuNCs. Therefore, the structural and hydration changes of ligand protein should be investigated emphatically. We monitor the pressure-induced conformational changes of BSA in AuNCs@BSA by using *in situ* IR spectra, as it is a valuable method to measure the changes in the secondary structure of proteins.[39] Figure 6 shows the pressure-dependent FT-IR spectra of BSA and those of AuNCs@BSA in D_2O. A band centered at 1653 cm^{-1} predominates in the amide I′ region of the native BSA in Figure 6A, being characteristic for the buried α-helix and its high contents. As shown, with pressure increase the band shifts to lower wavenumbers and gets broaden albeit no much intensity changes, which suggest a significant loss of the buried α-helix structure (vide infra). For the AuNCs@BSA, at atmospheric pressure, a major broad band at 1646 cm^{-1} is observed in Figure 6B, being somewhat different from those observed for native BSA in Figure 6A. Such a difference can be attributed to the variation of the protein structure during AuNCs@BSA synthesis, which indicates that both the extremely basic condition in the synthesis process of AuNCs@BSA and the consequently inclusion of AuNCs inside indeed change the secondary structure arrangement of BSA somewhat. With pressure increase, it can be observed that the amide I′ band increase obviously, and at the same time, it shifts slightly to the lower wavenumbers. More detailed analysis on the conformational changes are performed by plotting the maximum intensity of the amide I′ band vs pressure (inset in Figure 6B), where a drastic sigmoidal trend beginning from ∼100 MPa and indicating that the occurrence of big changes in the conformations of the albumin in the conjugates. However,

dx.doi.org/10.1021/jp309175k | J. Phys. Chem. C 2013, 117, 639−647

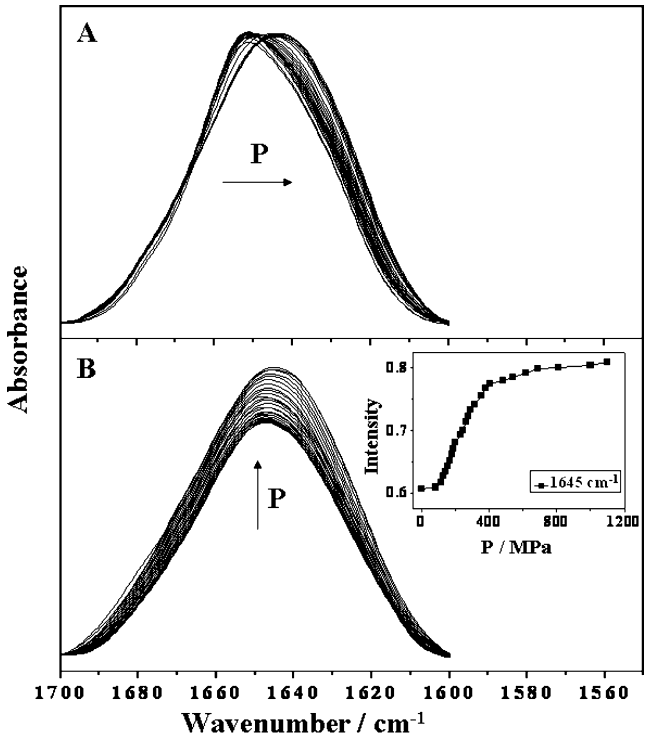

Figure 6. FT-IR spectra in the amide I′ region of (A) BSA and (B) AuNCs@BSA in D_2O, which are measured at various pressures from 0.1 to 1100 MPa. Arrow represents the direction of changes with pressure increase. Inset: the intensity changes of featuring band at 1645 cm^{-1} in FT-IR spectra vs pressure for AuNCs@BSA.

for the native BSA, such point starts at ~400 MPa,[40] implying that the metastable BSA in AuNCs@BSA is more sensitive to pressure than the native BSA.

In order to clarify more precisely the secondary structure changes of ligand BSA under pressure, we performed in Figure 7 the curve fitting for several representative IR spectra in Figure 6A,B, and the calculated proportions of the secondary structure elements are shown in Table 1. For the native BSA at ambient pressure in Figure 6A, the area percentages of the fitting Gaussian curves are 19.9, 46.6, 20.5, and 12.9% for the bands at 1629, 1654, 1640, and 1673 cm^{-1}, being assigned to characteristic for the exposed α-helix, the buried α-helix, random coil, and turn structures, respectively. Such contents are highly consistent with the reported structures of BSA[41,42] and, therefore, validate well both the spectral measurement and the curve-fitting methods we used. So we further apply the identical curve-fitting process to the IR spectra of BSA and AuNCs@BSA measured at other different pressures. For the AuNCs@BSA at ambient pressure, the secondary structural contents of BSA in it are evaluated as 28.2, 20.7, 28.2, and 22.9% for the exposed α-helix, buried α-helix, random coil, and turn structures, respectively. The structural contents, in particular the buried α-helix, are largely different from those observed for the native BSA, confirming again the metastable structures of BSA in packing with AuNCs. When the pressure is

Table 1. Fraction of Secondary Structure Elements of BSA and AuNCs@BSA in the Initial and Final Pressure States, Respectively

		percentages of secondary structure elements (%)			
protein	*P* (MPa)	exposed α-helix	buried α-helix	random	turn
BSA	0.1	19.9	46.6	20.5	12.9
	1000	31.7	27.4	27.6	13.3
AuNCs@BSA	0.1	28.2	20.7	28.2	22.9
	1000	31.9	32.1	17.3	18.7

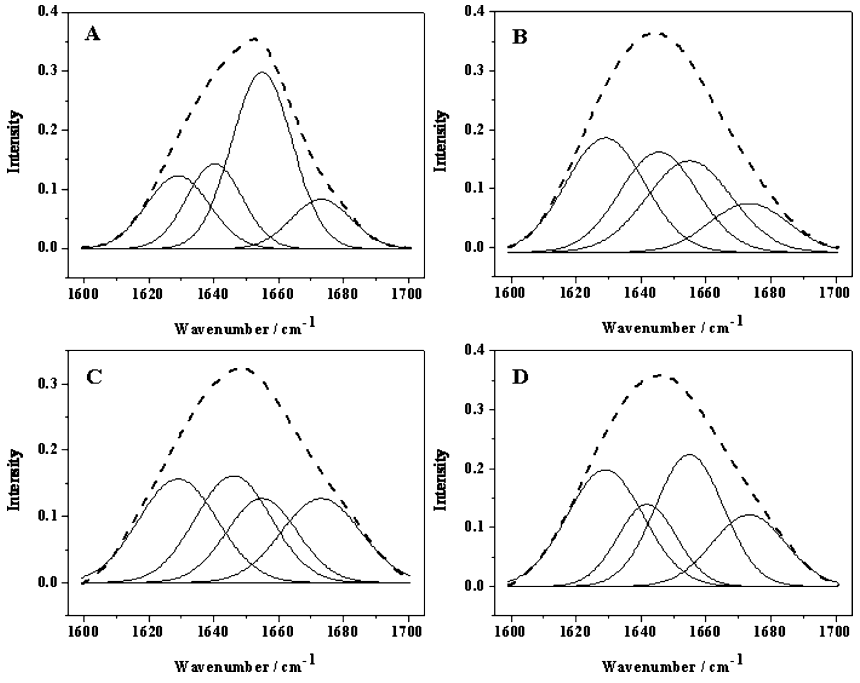

Figure 7. Curve fitting with Gaussian functions of the FT-IR spectrum of (A) initial state and (B) final state of BSA and (C) initial state and (D) final state of AuNCs@BSA in the pressure measurements. The dashed line represents the original spectrum for each case, while the solid lines represent the best fitted bands for individual component.

dx.doi.org/10.1021/jp309175k | J. Phys. Chem. C 2013, 117, 639−647

raised above 1000 MPa, the secondary structural elements of BSA in AuNCs@BSA have been rearranged. From Figure 6B and Table 1, it can be seen clearly that the percentages of both the exposed α-helix and the buried α-helix are increased, but the random coil and turn structures are decreased with pressure. That is, high pressure facilitates the acquisition of ordered structure in ligand BSA, being get closer to those observed for BSA at the identical pressure. It was reported that high hydrostatic pressure can increase protein folding by reducing the interactions among partially folded intermediates as well as the nonspecific aggregation.[43] The changes in chemical environment may induce electronic energy splitting and electron redistribution on the cluster surface, leading to a variation of the optical properties of the metal NCs.[44]

4. DISCUSSION

4.1. Large Differences of Secondary Structures Exist between BSA and AuNCs@BSA. From the results listed in Figure 3, Figure 7, and Table 1, we know the synthesis process of AuNCs at extremely basic condition and the following encapsulation of it in BSA have changed the secondary structures of BSA a little. In comparison to the native one, the BSA ligand in AuNCs@BSA contains more exposed α-helix (28.2% vs 19.9%), random coil (28.2% vs 20.5%), and turn structure (22.9% vs 12.9%) but much less buried α-helix (20.7% vs 46.6%). That is, the total amount of α-helix is decreased from 66.5% in native BSA to 48.9% in AuNCs@BSA, which is very close to that reported by Pradeep et al.[45] Such changes should be attributed to two related issues: first, the extremely basic conditions during synthesis, which denatured the protein completely albeit following dialysis was proposed to refold the protein, and second, the covalent bond between gold atom and electron-rich atoms (e.g., N, O) or groups (e.g., COOH, NH_2) in BSA[5,46] should break some as-existed bond of native BSA, which should change the tertiary and secondary structures of it a little.

In addition, it is note that the pressure-induced secondary structure changes of BSA ligand in AuNCs@BSA are obviously distinct from those of BSA, albeit both getting closer in final at high pressure. For AuNCs@BSA, the random coil and turn structures decrease but the buried and exposed α-helix increase with pressure, especially, more helical ordered structures appear at high pressure. In fact, the entrapped gold nanoclusters may change the unfolding pathway somewhat of the ligand BSA during compression, which suggest that the changing mechanism of AuNCs@BSA conformation may be different from the native BSA under pressure. Further investigation needs to be performed.

4.2. Origination of AuNCs@BSA Luminescence and Its Enhancement with Pressure. The luminescence of metal nanoparticles as gold and silver has long been an intriguing topic and has drawn considerable research interesting for some time.[2,11−16] Owing to the efficient nonradiative decay and the absence of an energy gap, generally the luminescence of metal is extremely weak.[47] However, recent studies indeed show that the small metal NCs can behave as "artificial atoms" and show photoluminescence with relative high QY,[2−4,48−50] which can be 7−9 orders of magnitude higher than that of bulk gold (10^{-10}).[2] With the rapid developments of both synthesis strategies and applications achieved recently, the luminescence properties of metal NCs have fascinated the scientific community, and currently several mechanisms have been proposed to explain the emission properties of the ultrasmall metal NCs.[12,51−53] Although, unlike QDs, no defined mechanism has already been known to explain the emission from all metal NCs, the studies indeed suggest two major sources are essential for the fluorescence of metal NCs. Following these investigations, we try to explore the luminescence origination of AuNCs@BSA by employing hydrostatic pressure as a perturbation, in particular to investigate the pressure effect on the conformational changes of ligand BSA in the bioconjugates. The fluorescence enhancements induced by pressure stands to reason in the present study, which is essentially an important discovery in monitoring and/or improving the luminescence QY of NCs. Although the mechanism of it cannot be defined at this moment, we tentatively propose two possibilities here for them: (1) with pressure the conformational changes of surrounding BSA change a lot of microenvironment of the gold core, leading to the changing of surface properties to a state favor the AuNCs@BSA luminance; (2) the arrangement of gold atoms in core is changed with pressure, which finally changed the gold(I)−gold(I) interactions. However, the second possibility is less likely occurring based on the views reported as follows.

The use of high-pressure study on homogeneous nanostructures was critically reviewed by San-Miguel,[23] where how pressure affects structuration or confinement on several nanocrystal systems was summarized, and it was concluded that the structural transformation of nanoclusters proceeded generally at pressure of ∼6 GPa or even higher. In addition, the compressibility of silver and gold nanoparticles suspended in a methanol−ethanol mixture was studied by X-ray diffraction with synchrotron radiation at pressures up to 30 GPa,[54] which demonstrated that the investigated nanoparticles were significantly stiffer than the corresponding bulk materials as no phase transformation or noncubic lattice distortions were observed in the investigated pressure range. Therefore, it can be concluded that the pressure-induced lattice rearrangement and/or distortion of gold core in AuNCs@BSA cannot occur at the pressure range low as we used (<1.1 GPa). Furthermore, because Au_{25} nanoclusters generally share a common Au_{13}/Au_{12} core−shell structure regardless of the types of ligands,[16] any structural changes of it should contribute a large luminescence shift.[55] The nonshift fluorescence observations in Figure 4 suggest that it cannot be attributed to the quantization effect of metal core. Rather, the pressure-induced conformational changes of protein ligand, especially, the interaction changes between the protein and the gold core, should play essential roles in the fluorescence enhancement of AuNCs.

4.3. Pressure-Induced Conformational Changes of BSA Favor the AuNCs@BSA Luminescence. Although the fluorescence of metal nanoparticles has drawn considerable research interest in the fields of chemistry, materials, and biology,[8,56,57] the studies of the surface ligands role on the fluorescence of gold nanoclusters are still limited.[13,36,53,58] Wang et al.[13,58] explored the effects of polar thiolate ligands on the NIR luminescence intensities of monolayer-protected Au_{38} and Au_{140} quantum dots. Exchanges of the initial phenylethanethiolates on Au_{38} MPCs and hexanethiolates on Au_{140} MPCs by new polar ligands result in increases in the near-infrared (NIR) luminescence intensities. The observations were consistent with sensitivity of the luminescence mechanism to any factor that enhances the electronic polarization of the bonds between the Au core atoms and their thiolate ligands. Wu and Jin[53] have investigated the fluorescence from $Au_{25}(SR)_{18}$ nanoclusters by correlating with several ligands with

dx.doi.org/10.1021/jp309175k | J. Phys. Chem. C 2013, 117, 639−647

distinguish properties. The results demonstrated that the surface ligand of $Au_{25}(SR)_{18}$ played a major role in fluorescence generation; in particular, ligands with electron-rich atoms (e.g., N, O) or groups (e.g., COOH, NH_2) can largely promote fluorescence. In addition, in that paper it also reported that another two factors, the electron donation capability of the ligands and the electropositivity of the metal core, were also very important in determining the fluorescence of gold core. The pressure-induced conformational changes of protein indeed relate these issues directly.

In general, the effect of pressure on protein structure favor states that exhibit a smaller specific volume because the pressure derivative of the Gibbs free energy change between two states is equal to their difference in volume. And generally the decrease in specific volume of proteins observed upon partial or complete unfolding of the native structure is caused by a combination of several effects:[59] (1) disruption of salt bridges, (2) hydration of newly exposed nonpolar and polar residues, and (3) the loss from packing defects in the completely folded structure. Essentially in protein, as the formations of ion pairs and hydrophobic bonds are generally accompanied by a large positive volume change,[60] the application of high pressures on protein in solutions should strongly disrupt the intramolecular electrostatic and hydrophobic interactions. Therefore, during high-pressure treatment, both the amino and carboxyl groups in proteins will become ionized, and simultaneously, the net charge of protein will be consequently increased, which may push the ligand donate more electron density to the metal core via the S−Au bond; i.e., the capability of ligand charge is increased. Furthermore, the pressure-induced disruption of hydrophobic interactions will leave more hydrophobic group free albeit being more hydrated, becoming more capable of pushing electron density to the sulfur atom and hence affects the Au core through the S−Au bond. In addition, the hydration of exposed groups should also play a decisive role on the AuNCs@BSA luminance and can therefore be regarded as an important factor for understanding the pressure-induced fluorescence enhancement. According to the related reports on molecular dynamics simulation, the surface water density (number of water molecules in the hydration shell divided by the surface area) increase with pressure, in particular around the nonpolar and negatively charged residues at the protein surface.[61] Both experimental and theoretical approaches indicate that the underlying mechanism of pressure unfolding is essentially to the penetration of water into the protein matrix.[59] Our observation of more exposed α-helix available at high pressure confirms this point, indicating that the fluorescence should be largely enhanced by the hydration of moieties released from pressure disruption of the intramolecular electrostatic and hydrophobic interactions.

In connection the AuNCs@BSA intensity of featuring band in FT-IR spectra to those observed in fluorescence spectra at various pressures (Figure 6 vs Figure 5), the relative infrared and fluorescence intensity are both increased under compression. However, it should be noted that the jumping-off point of pressure-induced intensity in FT-IR (inset in Figure 6) is not well consistent with that of fluorescence spectra (inset in Figure 4), as the former starts at quite low pressure (∼100 MPa) in comparison to that of the latter. This should be ascribed to that the emission characteristics of AuNCs@BSA actually reflected the total contributions of several factors of the conformational changes of BSA induced by pressure, while those of IR spectra reflect essentially the secondary structural changes of BSA. Being different from the intramolecular electrostatic and hydrophobic interactions in proteins, the formation of hydrogen bond is generally associated with small volume changes, and so it is less pressure sensitive. This means that while high-pressure treatment readily disrupts the tertiary and quaternary structure of globular proteins, generally it has less influence on the secondary structures. That is why, for some proteins in solution, pressure alone does not cause complete unfolding because of a small volume change or a large stability.[25,62] As such a stable globular protein of BSA,[63] at native state it does not lost its ordered structure much under compression: events mainly occur at the exchange from the buried α-helix to the exposed one (see Table 1). However, the results shown in Figure 6B and Table 1 for AuNCs@BSA indicate large secondary structures indeed occur with pressure. In AuNCs@BSA, BSA could adopt a more flexible state on the boundary surface of gold nanoclusters as a result of the conformational changes in the bioconjugation. So it can be concluded that at the low-pressure region the tertiary and quaternary structural changes, while at the high-pressure region the hydration of ligands and secondary structural changes play a crucial role in determining the fluorescence behavior of gold NCs.

Taking the discussion as a whole, we can infer that the pressure-induced disruption of salt bridges, the enhanced hydration of newly exposed nonpolar and polar residues, and especially the disruption of hydrophobic interactions are the important factors for the fluorescence enhancement of gold core. These results are in agreement with the findings reported previously for the small molecule-protected luminescent gold nanoclusters.[13,53,58]

4.4. Strong Binding between BSA and AuNCs Prevents the Pressure-Induced BSA Unfolding. The most important finding is that complexation with AuNCs protects the globular protein against aggregation caused by intermolecular −SS− bond during high-pressure processing. This protective effect may be due, in part at least, to the blocking of the −SH in the protein by the binding with gold core. Size exclusion chromatography indicated extensive pressure-induced protein unfolding and aggregation during BSA treatment at 400 MPa, and furthermore, the decrease and increase of total and exposed −SH groups, respectively, were enhanced by pressure above 500 MPa.[64] The strong protein aggregation was considered to be mainly due to formation of intermolecular disulfide bridges via −SH/−SS− interchange.[65] However, in AuNCs@BSA, the ligand protein is proposed to connect with the AuNCs core partially through a covalent linkage of Au−S bond.[2,37,66] The strong binding between Au−S, that is, the occupation of −SH in BSA by AuNCs, should prevent the rapid denaturation of the partially unfolded protein with gold core and protect it against protein−protein aggregation.

It seems likely that these pressure-induced BSA aggregates are stabilized by disulfide linkages, since BSA (like β-lactoglobulin) has a free cysteine residue which, under appropriate conditions in the partly unfolded molecule, can become available for intermolecular association with other sulfhydryl or disulfide groups. Earlier work[65] has demonstrated that there is a loss of more than half of the free sulfhydryl groups during treatment at 800 MPa for 20 min and that dithiothreitol (DTT) addition reduces these units to monomer status in the pressure-treated samples. The well-folded global

dx.doi.org/10.1021/jp309175k | J. Phys. Chem. C 2013, 117, 639−647

proteins are packed tightly together via electrostatic and hydrophobic interactions as well as hydrogen bonding. This may not be the case for AuNCs@BSA bioconjugates during the pressure treatment since it is known that ionic bonds are disrupted under high pressure. Hence, we may speculate that the application of high pressure leads to dissociation of the electrostatic interaction in the native BSA; whereupon the protein becomes partially denatured in AuNCs@BSA bioconjugates, a manner may differ somewhat from the pressure-induced denaturation of the BSA alone. The gain of more helical ordered structures at high pressure (from 48.9% to 64% of α-helix in total) validates this speculation well.

5. CONCLUSIONS

Pressure-induced fluorescence enhancements of AuNCs@BSA are investigated in the present study. On the basis of the combined experimental information presented in this paper, we can conclude that it is the protected ligand other than the core rearrangement that plays a major role for the fluorescence enhancement of AuNCs@BSA. BSA adopts a more flexible conformational state at the boundary surface of AuNCs as a result of different conformational changes way in the bioconjugates from native BSA. The pressure-induced disruption of salt bridges, the enhanced hydration of newly exposed nonpolar and polar residues, and especially the disruption of hydrophobic interactions of ligand influence the optical property of gold nanoclusters greatly. Albeit these results are in agreement with the findings reported previously for the small molecule-protected luminescent gold nanoclusters,[52,57,57] the present study still lays the foundation for improving the NCs luminescence by adjusting the conformation of protein ligand. In addition, the reported environment-sensitive optical properties of metal NCs have enabled the development of new techniques for sensitive chemical and biological sensing.

AUTHOR INFORMATION

Corresponding Author

*Tel +86-431-85168730 (Y.W.); Fax +86-431-85193421 (Y.W.); e-mail yqwu@jlu.edu.cn (Y.W.), zoubo@jlu.edu.cn (B.Z.).

Notes

The authors declare no competing financial interest.

ACKNOWLEDGMENTS

The present work was supported by the projects of NSFC (Nos. 20934002, 20973073, 91027027, and 21003061) and the State Key Laboratory of Supramolecular Structure and Materials, Jilin University.

REFERENCES

(1) Xavier, P. L.; Chaudhari, K.; Baksi, A.; Pradeep, T. *Nano Rev.* **2012**, *3*, 14767−14783.
(2) Shang, L.; Dong, S.; Nienhaus, G. U. *Nano Today* **2011**, *6*, 401−418.
(3) Pei, Y.; Zeng, X. C. *Nanoscale* **2012**, *4*, 4054−4072.
(4) Maity, P.; Xie, S.; Yamauchiab, M.; Tsukuda, T. *Nanoscale* **2012**, *4*, 4027−4037.
(5) Xie, J.; Zheng, Y.; Ying, J. Y. *J. Am. Chem. Soc.* **2009**, *131*, 888−889.
(6) Richards, C. I.; Choi, S.; Hsiang, J. C.; Antoku, Y.; Vosch, T.; Bongiorno, A.; Tzeng, Y. L.; Dickson, R. M. *J. Am. Chem. Soc.* **2008**, *130*, 5038−5039.
(7) Yu, J. H.; Choi, S.; Dickson, R. M. *Angew. Chem., Int. Ed.* **2009**, *48*, 318−320.
(8) Lin, C. A. J.; Yang, T. Y.; Lee, C. H.; Huang, S. H.; Sperling, R. A.; Zanella, M.; Li, J. K.; Shen, J. L.; Wang, H. H.; Yeh, H. I.; et al. *ACS Nano* **2009**, *3*, 395−401.
(9) Muhammed, M. A. H.; Pradeep, T. *Adv. Fluoresc. Rep. Chem. Biol. II* **2010**, *9*, 333−353.
(10) Retnakumari, A.; Setua, S.; Menon, D.; Ravindran, P.; Muhammed, H.; Pradeep, T.; Nair, S.; Koyakutty, M. *Nanotechnology* **2010**, *21* (055103), 12.
(11) Bigioni, T. P.; Whetten, R. L. *J. Phys. Chem. B* **2000**, *104*, 6983−6986.
(12) Link, S.; Beeby, A.; FitzGerald, S.; El-Sayed, M. A.; Schaaff, T. G.; Whetten, R. L. *J. Phys. Chem. B* **2002**, *106*, 3410−3415.
(13) Wang, G.; Huang, T.; Murray, R. W.; Menard, L.; Nuzzo, R. G. *J. Am. Chem. Soc.* **2005**, *127*, 812−813.
(14) Parker, J. F.; Fields-Zinna, C. A.; Murray, R. W. *Acc. Chem. Res.* **2010**, *43*, 1289−1296.
(15) Varnavski, O.; Ramakrishna, G.; Kim, J.; Lee, D.; Goodson, T. *J. Am. Chem. Soc.* **2010**, *132*, 16−17.
(16) Wen, X.; Yu, P.; Toh, Y.; Tang, J. *J. Phys. Chem. C* **2012**, *116*, 11830−11836.
(17) Wang, Q.; Li, S.; He, L.; Qian, Y.; Li, X.; Sun, W.; Liu, M.; Li, J.; Li, Y.; Yang, G. *ChemPhysChem* **2008**, *9*, 1146−1152.
(18) Drickamer, H. G. *J. Lumin., Part I* **1991**, *48*−*49*, 11−17.
(19) Giepmans, B. N. G.; Adams, S. R.; Ellisman, M. H.; Tsien, R. Y. *Science* **2006**, *312*, 217−224.
(20) Wiedenmann, J.; Nienhaus, G. U. *Expert Rev. Proteomics* **2006**, *3*, 361−374.
(21) Nienhaus, G. U.; Wiedenmann, J. *ChemPhysChem* **2009**, *10*, 1369−1379.
(22) Tolbert, S. H.; Herhold, A. B.; Brus, L. E.; Alivisatos, A. P. *Phys. Rev. Lett.* **1996**, *76*, 4384−4387.
(23) San-Miguel, A. *Chem. Soc. Rev.* **2006**, *35*, 876−889.
(24) Jacobs, K.; Wickham, J.; Alivisatos, A. P. *J. Phys. Chem. B* **2002**, *106*, 3759−3762.
(25) Jacobs, K.; Zaziski, D.; Scher, E. C.; Herhold, A. B.; Alivisatos, A. P. *Science* **2001**, *293*, 1803−1806.
(26) Li, H. W.; Ai, K.; Wu, Y. *Chem. Commun.* **2011**, *47*, 9852−9854.
(27) Czarnik-Matusewicz, B.; Murayama, K.; Wu, Y.; Ozaki, Y. *J. Phys. Chem. B* **2000**, *104*, 7803−7811.
(28) Murayama, K.; Wu, Y.; Czarnik-Matusewicz, B.; Tsenkova, R.; Ozaki, Y. *J. Phys. Chem. B* **2001**, *105*, 4763−4769.
(29) Moulder, J. F.; Stickle, W. F.; Sobol, P. E.; Bomben, K. D. *Handbook of X-ray Photoelectron Spectroscopy*; Perkin-Elmer Corp.: Eden Prairie, MN, 1992.
(30) Huang, C. C.; Liao, H. Y.; Shiang, Y. C.; Lin, Z. H.; Yang, Z.; Chang, H. T. *J. Mater. Chem.* **2009**, *19*, 755−759.
(31) Muhammed, M.; Verma, P.; Pal, S.; Kumar, R.; Paul, S.; Omkumar, R.; Pradeep, T. *Chem.—Eur. J.* **2009**, *15*, 10110−10120.
(32) Negishi, Y.; Nobusada, K.; Tsukuda, T. *J. Am. Chem. Soc.* **2005**, *127*, 5261−5270.
(33) Zhu, M.; Lanni, E.; Garg, N.; Bier, M. E.; Jin, R. *J. Am. Chem. Soc.* **2008**, *130*, 1138−1139.
(34) Mohanty, J. S.; Xavier, P. L.; Chaudhari, K.; Bootharaju, M. S.; Goswami, N.; Pal, S. K.; Pradeep, T. *Nanoscale* **2012**, *4*, 4255−4262.
(35) Liu, H.; Zhang, X.; Wu, X.; Jiang, L.; Burda, C.; Zhu, J. *Chem. Commun.* **2011**, *47*, 4237−4239.
(36) Shang, L.; Brandholt, S.; Stockmar, F.; Trouillet, V.; Bruns, M.; Nienhaus, G. U. *Small* **2012**, *8*, 661−665.
(37) Xavier, P. L.; Chaudhari, K.; Verma, P. K.; Pal, S. K.; Pradeep, T. *Nanoscale* **2010**, *2*, 2769−2776.
(38) Noda, I.; Ozaki, Y. *Two-Dimensional Correlation Spectroscopy - Applications in Vibrational and Optical Spectroscopy*; Wiley: New York, 2004.
(39) Mantsch, H. H.; Chapman, D. *Infrared Spectroscopy of Biomolecules*; Wiley: New York, 1996.
(40) Zhang, M.; Wu, Y. *Anal. Sci.* **2011**, *27*, 1139−1142.
(41) Harris, P. I.; Chapman, D. *Biopolymers* **1995**, *37*, 251−263.

(42) Meersman, F.; Smeller, L.; Heremans, K. *Biophys. J.* **2002**, *82*, 2635−2644.
(43) Gorovits, B. M.; Horowitz, P. M. *Biochemistry* **1998**, *37*, 6132−6135.
(44) Zhou, R.; Shi, M.; Chen, X.; Wang, M.; Chen, H. *Chem.—Eur. J.* **2009**, *15*, 5436−5440.
(45) Muhammed, M. A. H.; Verma, P. K.; Pal, S. K.; Retnakumari, A.; Koyakutty, M.; Nair, S.; Pradeep, T. *Chem.—Eur. J.* **2010**, *16*, 10103−10112.
(46) Wei, H.; Wang, Z.; Zhang, J.; House, S.; Gao, Y.-G.; Yang, L.; Robinson, H.; Tan, L. H.; Xing, H.; Hou, C.; et al. *Nat. Nanotechnol.* **2010**, *280*, 93−97.
(47) Mooradian, A. *Phys. Rev. Lett.* **1969**, *22*, 185−187.
(48) Sharma, J.; Yeh, H. C.; Yoo, H.; Werner, J. H.; Martinez, J. S. *Chem. Commun.* **2011**, *47*, 2294−2296.
(49) Zheng, J.; Petty, J. T.; Dickson, R. M. *J. Am. Chem. Soc.* **2003**, *125*, 7780−7781.
(50) Jao, Y. C.; Chen, M. K.; Lin, S. Y. *Chem. Commun.* **2010**, *46*, 2626−2628.
(51) Huang, C. C.; Hung, Y. L.; Shiang, Y. C.; Lin, T. Y.; Lin, Y. S.; Chen, C. T.; Chang, H. T. *Chem.—Asian J.* **2010**, *5*, 334−341.
(52) Zhou, C.; Sun, C.; Yu, M.; Qin, Y.; Wang, J.; Kim, M.; Zheng, J. *J. Phys. Chem. C* **2010**, *114*, 7727−7732.
(53) Wu, Z.; Jin, R. *Nano Lett.* **2010**, *10*, 2568−2573.
(54) Gu, Q. F.; Krauss, G.; Steurer, W.; Gramm, F.; Cervellino, A. *Phys. Rev. Lett.* **2008**, *100* (045502), 4.
(55) Wu, Z.; Gayathri, C.; Gil, R. R.; Jin, R. *J. Am. Chem. Soc.* **2009**, *131*, 6535−6542.
(56) Peyser, L. A.; Vinson, A. E.; Bartko, A. P.; Dickson, R. M. *Science* **2001**, *29*, 103−106.
(57) Tang, Z.; Xu, B.; Wu, B.; Germann, M. W.; Wang, G. *J. Am. Chem. Soc.* **2010**, *132*, 3367−3374.
(58) Wang, G.; Guo, R.; Kalyuzhny, G.; Choi, J.; Murray, R. W. *J. Phys. Chem. B* **2006**, *110*, 20282−20289.
(59) Silva, J. L.; Foguel, D.; Royer, C. A. *Trends Biochem. Sci.* **2001**, *26*, 612−618.
(60) Masson, P. Pressure Denaturation of Proteins. In *High Pressure and Biotechnology*; Balny, C., Hayashi, R., Heremans, K., Masson, P., Eds.; Colloque INSERM/John Libbey Eurotext Ltd.: Montrouge, France, 1992; Vol. *224*, pp 89−99.
(61) Smolin, N.; Winter, R. *Biochim. Biophys. Acta* **2006**, *1764*, 522−534.
(62) Silva, J. L.; Foguel, D.; Dapoian, A. T.; Prevelige, P. E. *Curr. Opin. Struct. Biol.* **1996**, *6*, 166−175.
(63) Hayakawa, I.; Kajihara, J.; Morikawa, K.; Oda, M.; Fujio, Y. *J. Food Sci.* **1992**, *57*, 288−292.
(64) Galazka, V. B.; Ledward, D. A.; Sumner, I. G.; Dickinson, E. *J. Agric. Food Chem.* **1997**, *45*, 3465−3471.
(65) Galazka, V. B.; Sumner, I. G.; Ledward, D. A. *Food Chem.* **1996**, *57*, 393−398.
(66) Chaudhari, K.; Xavier, P. L.; Pradeep, T. *ACS Nano* **2011**, *5*, 8816−8827.